Fluorescent Porous Polymer Films as TNT Chemosensors: Electronic and Structural Effects

Jye-Shane Yang and Timothy M. Swager*

Contribution from the Department of Chemistry, Massachusetts Institute of Technology, 77 Massachusetts Ave., Cambridge, Massachusetts 02139

Received June 30, 1998

Abstract: The synthesis, spectroscopy, and fluorescence quenching behavior of pentiptycene-derived phenyleneethynylene polymers, **1**−**3**, are reported. The incorporation of rigid three-dimensional pentiptycene moieties into conjugated polymer backbones offers several design advantages for solid-state (thin film) fluorescent sensory materials. First, they prevent π-stacking of the polymer backbones and thereby maintain high fluorescence quantum yields and spectroscopic stability in thin films. Second, reduced interpolymer interactions dramatically enhance the solubility of polymers **1**−**3** relative to other poly(phenyleneethynylenes). Third, the cavities generated between adjacent polymers are sufficiently large to allow diffusion of small organic molecules into the films. These advantages are apparent from comparisons of the spectroscopic and fluorescence quenching behavior of **1**−**3** to a related planar electron-rich polymer **4**. The fluorescence attenuation (quenching) of polymer films upon exposure to analytes depends on several factors, including the exergonicity of electron transfer from excited polymer to analytes, the binding strength (polymer-analyte interactions), the vapor pressure of the analyte, and the rates of diffusion of the analytes in the polymer films. Films of **1**−**3** are particularly selective toward nitro-aromatic compounds. The dependence of fluorescence quenching on film thickness provides an additional criterion for the differentiation of nitro-aromatic compounds from other species, such as quinones. In short, thinner films show a larger response to nitro-aromatic compounds, but show a lower response to quinones. Such differences are explained in terms of polymer−analyte interactions, which appear to be electrostatic in nature. The rapid fluorescence response (quenching) of the spin-cast films of **1**−**3** to nitro-containing compounds qualifies these materials as promising TNT chemosensory materials.

Introduction

New approaches to the detection of ultra-trace analytes are a central challenge in the field of chemical sensors.[1] Detection sensitivity has been principally determined by the transduction method (e.g. absorption, fluorescence, conductivity, etc.), and the design of new materials has been focused upon endowing selectivity. Polymeric materials can provide selectivity from their intrinsic nature (e.g. polar or nonpolar, aromatic or hydrocarbon, etc.), functional groups, and the presence of well-defined receptors. However, the ultimate materials for chemical sensors will need to satisfy additional criteria, including the ability to amplify a transduction event, a high stability to temperature and/or solvents, and an easily measurable transduction signal.

Our group has been investigating a variety of approaches that utilize the special transport properties of conjugated polymers to enhance transduction signals resulting from analyte binding.[2] In fluorescence-based sensor schemes, facile energy migration processes intrinsic to conjugated polymers are used to amplify signals. The initial demonstrations of this approach were made in dilute solutions of poly(phenyleneethynylenes) which had integrated receptor units.[3] In solution, the energy migration was necessarily restricted to a single polymer chain. Most fluorescence sensory devices, however, will require polymers to be immobilized on a solid support. In principle, although the greater tendency for energy migration in solids should provide even higher gain, in most conjugated polymer systems this advantage is countered by a decreased fluorescence quantum yield.[4] An additional problem is that dense polymer films can also prevent rapid diffusion of analytes into the material. To address these limitations, we recently developed a polymer that forms spectroscopically stable (reproducible) and highly fluorescent thin films. The key feature was the incorporation of rigid three-dimensional pentiptycene moieties in the polymer backbone that prevent π-stacking or excimer formation.[5] Our studies thus far have focused on developing sensors for 2,4,6-trinitrotoluene (TNT) and 2,4-dinitrotoluene (DNT), which are principal constituents of ca. 120 million unexploded land mines worldwide.[6] The obviously enormous problem of ridding the world of land mines is complicated by inefficient land mine detection using metal detectors due to the large number of false alarms. In this context, methods of direct TNT detection, including neutron activation analysis, electron capture detection, ion mobility spectrometry, and biosensors have been sought for better land mine detection.[6,7] However, there still exists a need for real-time TNT chemosensory devices that not only complement existing methods, but also provide the advantages of low cost and instrumental simplicity.

(1) (a) *Chemosensors of Ion and Molecule Recognition*; Desvergne, J. P., Czarnik, A. W., Eds.; Kluwer Academic Publishers: Boston, 1997. (b) de Silva, A. P.; Gunaratne, H. Q. N.; Gunnlaugsson, T.; Huxley, A. J. M.; McCoy, C. P.; Rademacher, J. T.; Rice, T. E. *Chem. Rev.* **1997**, *97*, 1515.
(2) Swager, T. M. *Acc. Chem. Res.* **1998**, *31*, 201 and references therein.
(3) Zhou, Q.; Swager, T. M. *J. Am. Chem. Soc.* **1995**, *117*, 12593.
(4) Jenekhe, S. A.; Osaheni, J. A. *Science* **1994**, *265*, 765.
(5) Yang, J.-S.; Swager, T. M. *J. Am. Chem. Soc.* **1998**, *120*, 5321.
(6) Maureen, R. A. *C&EN News* **1997**, *March 10*, 14.
(7) Kolla, P. *Angew. Chem., Int. Ed. Engl.* **1997**, *36*, 800.

10.1021/ja982293q CCC: $15.00
Published on Web 11/11/1998

Scheme 1

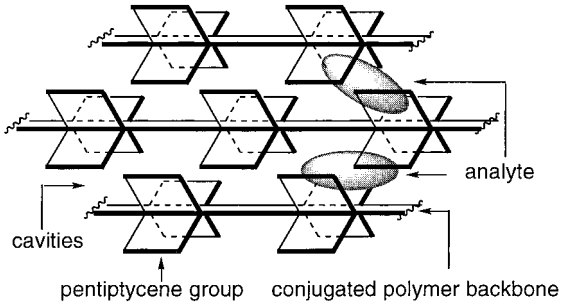

Chart 1

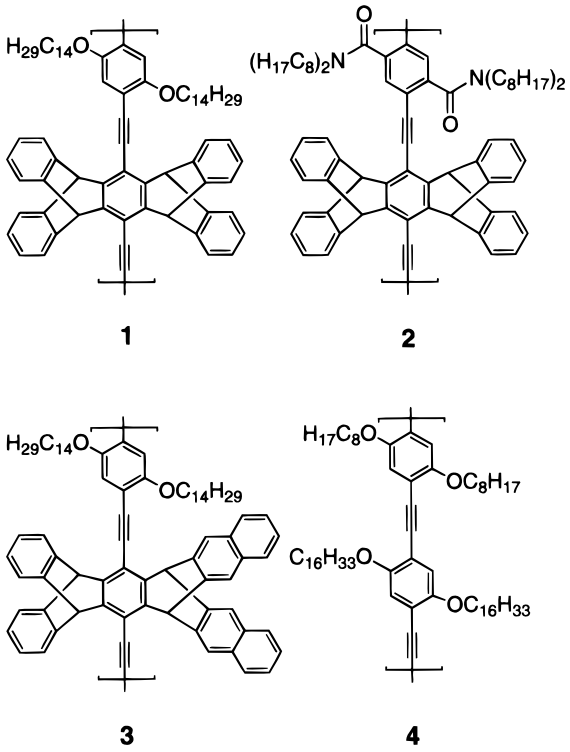

The fluorescence of the pentiptycene-derived polymer **1** in spin-cast films responds rapidly (seconds) to the vapors of TNT and DNT. We believe that the nonbonding electrostatic interactions[8] between the electron-rich polymer and the electron-deficient TNT or DNT molecules are critical in the rapid response processes to these analytes. The superior sensitivity of **1** in comparison to an electron-rich model polymer **4** also verifies the important role of film porosity. The porosity, shown conceptually in Scheme 1, is a result of the rigid pentiptycene groups, which provide cavities for analyte binding. We report herein our detailed studies of polymers **1**−**4** that probe the electronic and structural effects on fluorescence quenching with a variety of analytes. In comparison to polymer **1**, the electron-withdrawing character of amide substituents in polymer **2** provides a less electron-rich polymer backbone, whereas the extended pentiptycene structure of polymer **3** creates different thin film morphology while maintaining a polymer backbone with similar electronic properties to polymer **1**. Our results further suggest that both the electronic properties and the cavity size of polymer films are crucial determinants of fluorescence sensitivity toward TNT and DNT. We conclude that more electron-rich polymers and larger cavities will produce a larger fluorescence response to TNT and DNT.

Results and Discussion

Synthesis. The pentiptycene-derived polymers **1**−**3** are produced by palladium-catalyzed cross-coupling[9] of corresponding disubstituted diiodobenzenes (**5**[10] and **6**[3]) and pentiptycene diacetylenes (**7** and **8**) (eqs 1 and 2). Our synthesis of pentiptycene diacetylenes involves the pentiptycene quinones[11−16] (**10** and **11**), which are, in turn, obtained from the reaction of benzoquinone and anthracene or pentacene. The synthesis of polymer **4** has been reported elsewhere.[10]

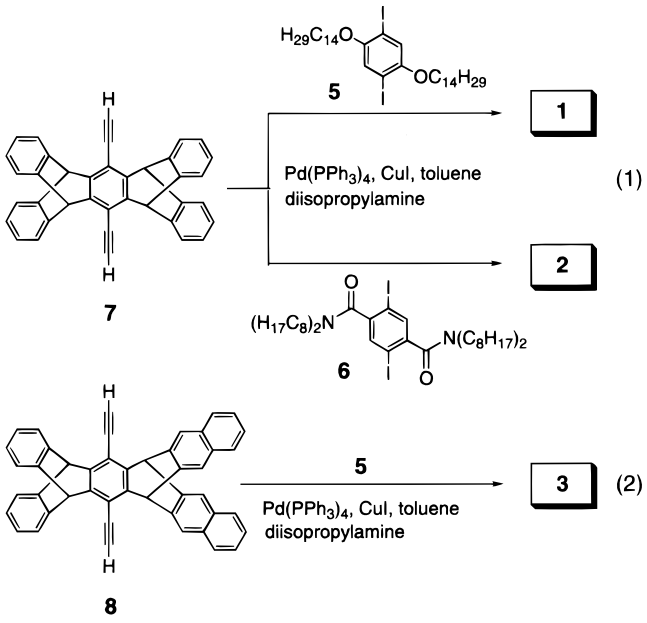

The first synthesis of **10** was carried out by Clar in 1931 using sequential Diels−Alder reactions of 1,4-benzoquinone and anthracene.[11] An alternate double Diels−Alder approach, with a 2:1 ratio of anthracene and 1,4-benzoquinone at room temperature in the presence of aluminum chloride catalyst, was reported in 1960.[12] The one-step formation of **10** directly from anthracene and 1,4-benzoquinone at 165 °C was also reported in the same year by Theilacker et al.[13] Another approach to **10** by Hart used a multistep synthesis starting with tetrabromohydroquinone dimethyl ether, anthracene, and *n*-butyllithium.[14] We performed the Diels−Alder reaction under conditions similar to those described by Theilacker and found, instead of **10**, the reaction produced a mixture of mono- and bis-adduct of hydroquinone species (eq 3) with poor solubility in organic solvents. These products were then converted to corresponding quinone products, **9** and **10**, by potassium bromate in acetic acid.[15]

(8) For recent discussion of aromatic electrostatic interactions see: (a) Cozzi, F.; Ponzini, F.; Annunziata, R.; Cinquini, M.; Siegel, J. S. *Angew. Chem., Int. Ed. Engl.* **1995**, *34*, 1019. (b) Williams, V. E.; Lemieux, R. P.; Thatcher, G. R. J. *J. Org. Chem.* **1996**, *61*, 1927.

(9) Heck, R. F. *Palladium Reagents in Organic Syntheses*; Academic Press: Orlando, 1985.

(10) Swager, T. M.; Gil, C. J.; Wrighton, M. S. *J. Phys. Chem.* **1995**, *99*, 4886.

(11) Clar, E. *Chem. Ber.* **1931**, *64*, 1676.

(12) Yates, P.; Eaton, P. *J. Am. Chem. Soc.* **1960**, *82*, 4436.

(13) Theilacker, W.; Berger-Brose, U.; Beyer, K.-H. *Chem. Ber.* **1960**, *93*, 1658.

(14) Hart, H.; Shamouilian, S.; Takehira, Y. *J. Org. Chem.* **1981**, *46*, 4427.

(15) Bartlett, P. D.; Ryan, M. J.; Cohen, S. G. *J. Am. Chem. Soc.* **1942**, *64*, 2649.

(16) Brodskii, A. I.; Gordienko, L. L.; Chukhlantseva, A. G.; Balandin, A. A.; Alieva, R. Y.; Klabunovskii, E. I.; Antik, L. V. *J. Struct. Chem. (Engl. Transl.)* **1970**, *11*, 564.

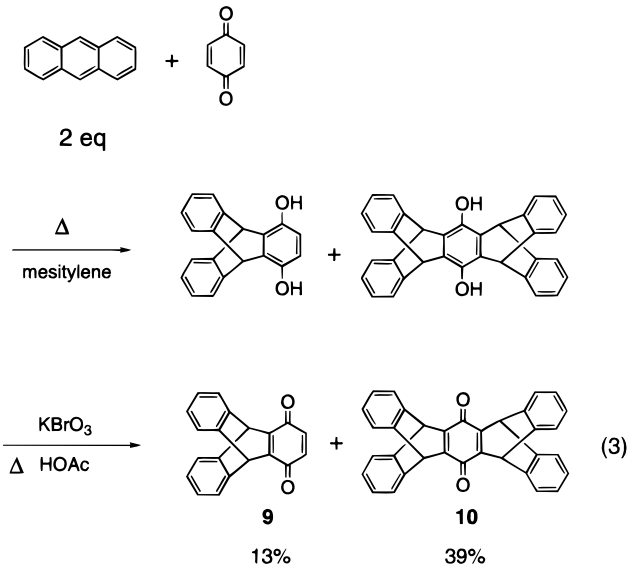

(3)

Quinone **11**[16] along with two characterized side products (**12** and **13**) were produced from a Diels−Alder reaction of **9** and pentacene in refluxing xylene solution followed by tautomerization and oxidation (eq 4). The assignment of a *cis* geometry

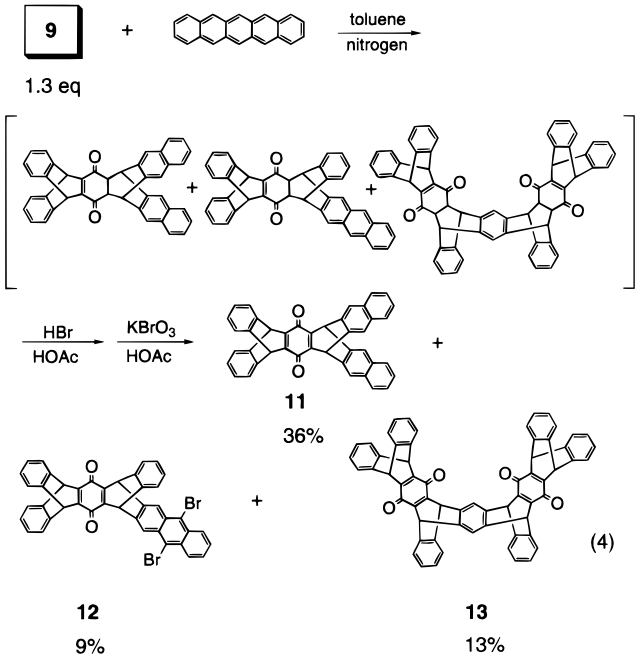

(4)

for **13** is based on the upfield shifts of characteristic bridgehead protons and the "inner" phenyl protons as compared to other iptycene quinones **9**−**12**. The relative ratio of **12** and **13** depends on the stoichiometry of starting materials (e.g. <10% of **13** was formed at 1:1 mole ratio).

Nucleophilic addition of lithium trimethylsilylacetylnide to quinone **10** followed by reductive aromatization of the central ring produced the trimethylsilyl-protected diethynylpentiptycene **14** (eq 5). Proton NMR spectroscopy showed the intermediate diol product to be a 1:1 *trans/cis* mixture. A single-crystal X-ray structure determination confirmed the pentiptycene structure of **14** (Figure 1). It is interesting to note that **14** exhibits clathrate behavior, with two methylene chloride solvent molecules occupying the cavities between adjacent pentiptycenes. Such an observation is also in agreement with the tendency of iptycene

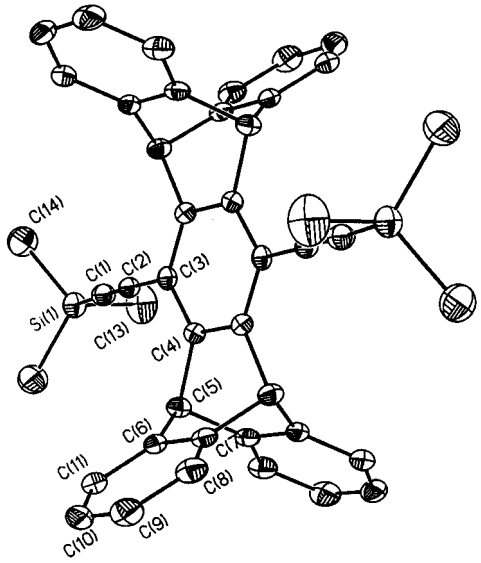

Figure 1. A single-crystal X-ray ORTEP (30% probability) structure of **14**.

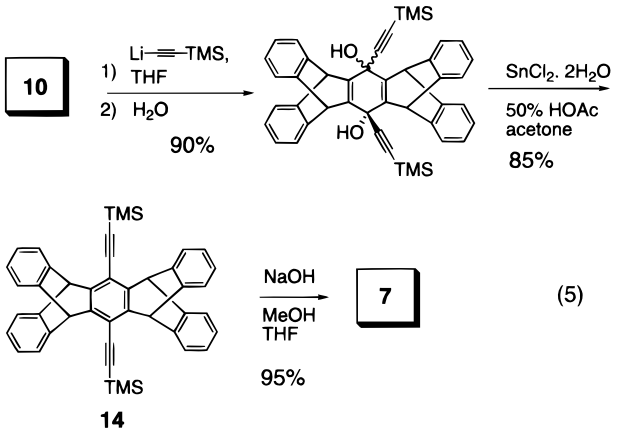

(5)

derivatives to form cavities in the solid state.[17] Deprotection of the TMS group provided the desired monomer **7**, which exhibits poor solubility in organic solvents. Similar chemistry applied to the quinone **11** provides the corresponding pentiptycene diacetylene **8** (eq 6), which has slightly better solubility than **7**, presumably due to a non-C_2 symmetric structure that results in less efficient packing in the solid state.

The molecular weights and polydispersity indices of polymers **1**−**4** determined by GPC are listed in Table 1. In contrast to the poor solubility of monomers **7** and **8**, the rigid-rod polymers **1**−**3** show exceptionally high solubility in organic solvents, such as chloroform, toluene, and tetrahydrofuran. This feature is attributed to the ability of the pentiptycene moieties to prevent π-stacking of conjugated polymer backbones thereby weakening the interpolymer interactions (vide infra). This unusual solubility property, wherein the polymer has better solubility than its monomer (or oligomers), tends to produce high PDIs and low molecular weight tails on the GPC trace for pentiptycene-derived polymers. The significantly reduced solubility of polymer **3** in comparison to **1** and **2** may account for its lower molecular weight than **1**. To elucidate the possible effect of polymer chain length on the sensitivity to TNT, a lower molecular weight sample of **1** was synthesized by performing the polymerization under dilute conditions.

(17) (a) Bashir-Hashemi, A.; Hart, H.; Ward, D. L. *J. Am. Chem. Soc.* **1986**, *108*, 6675. (b) Venugopalan, P.; Bürgi, H.-B.; Frank, N. L.; Baldridge, K. K.; Siegel, J. S. *Tetrahedron Lett.* **1995**, *36*, 2419. (c) Wilcox, C. F.; Roberts, F. D. *J. Org. Chem.* **1965**, *30*, 1959.

Table 1. Polymer Molecular Weight and Photophysical Data[a]

polymer	GPC M_n (PDI)	media[b]	abs λ_{max} (nm)[c]	fluo λ_{max} (nm)[c]	Φ_F[b]	τ (ns) (λ_{cx}, λ_{cm})
1	144 000 (2.6)	CH_2Cl_2	441	457	0.50	0.51 (420, 460)
		film	448	460	0.33	0.09 (440, 460)
	43 000 (6.0)					
2	34 000 (3.1)	CH_2Cl_2	372	421	0.61	0.47 (360, 420)
		film	370	423	0.42	0.05 (385, 425)
3	36 000 (7.9)	CH_2Cl_2	441	459	0.33	0.51 (420, 463)
		film	431	463, 497	0.76	0.05 (420, 463)
						0.49 (430, 500)
4	33 000 (4.7)	CH_2Cl_2	453	478	0.27	0.54 (430, 475)
		film	483	496	0.09	

[a] See Experimental Section for details of experimental conditions. [b] The thickness of films of polymers **1**−**3** are 200 Å and films of **4** are 30 Å. [c] The values of absorption and fluorescence maxima of **1**−**3** in 25-Å films are essentially the same as those of the corresponding 200-Å films.

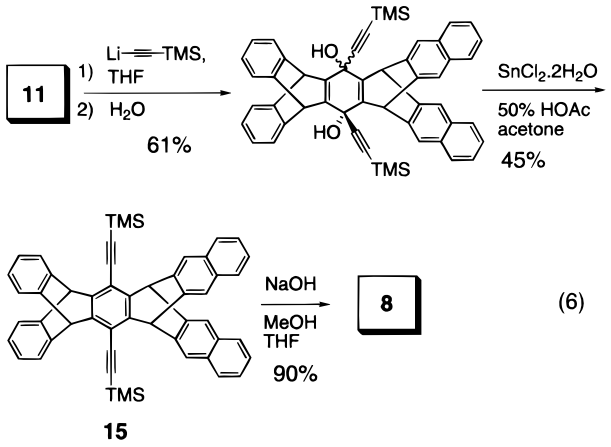

Absorption and Fluorescence Spectra. The absorption and fluorescence spectra of polymers **1**−**4** in dichloromethane and spin-cast films are shown in Figure 2. The corresponding photophysical data are reported in Table 1. The thickness of selected films was determined by ellipsometry and was correlated with the optical density. In comparison to **1**, polymer **2** absorbs and emits at a shorter wavelength with a larger Stokes shift and fluorescence bandwidth, which suggests a less ordered, and hence less conjugated, equilibrium polymer conformation resulting from the sterics of the amide groups.[18] We find that polymerizations to form **2** generally yield lower M_n values than those for **1**, which has led us to postulate that the increased sterics in **2** may also limit the efficiency of the polymerization reaction. The extremely similar spectroscopic properties of thin films and solutions of the polymers **1** and **2** also suggest very weak interpolymer electronic interactions.

In dichloromethane solution, **3** has absorption and fluorescence spectra similar to those of **1**. However in thin films, **3** displays a new broad band with a maximum at longer wavelengths in addition to a sharp 0−0 band. The relative fluorescence intensity of the broad vs sharp band depends on the film thickness and is larger in thicker films (Figure 2C). Dramatically different fluorescence lifetimes were obtained (Table 1) for emission wavelengths monitored at the maxima of broad and sharp bands. The lifetime at the sharp band is short and is comparable to those of **1** and **2** in films, while the broad band has a lifetime almost 10 times longer. Additionally,

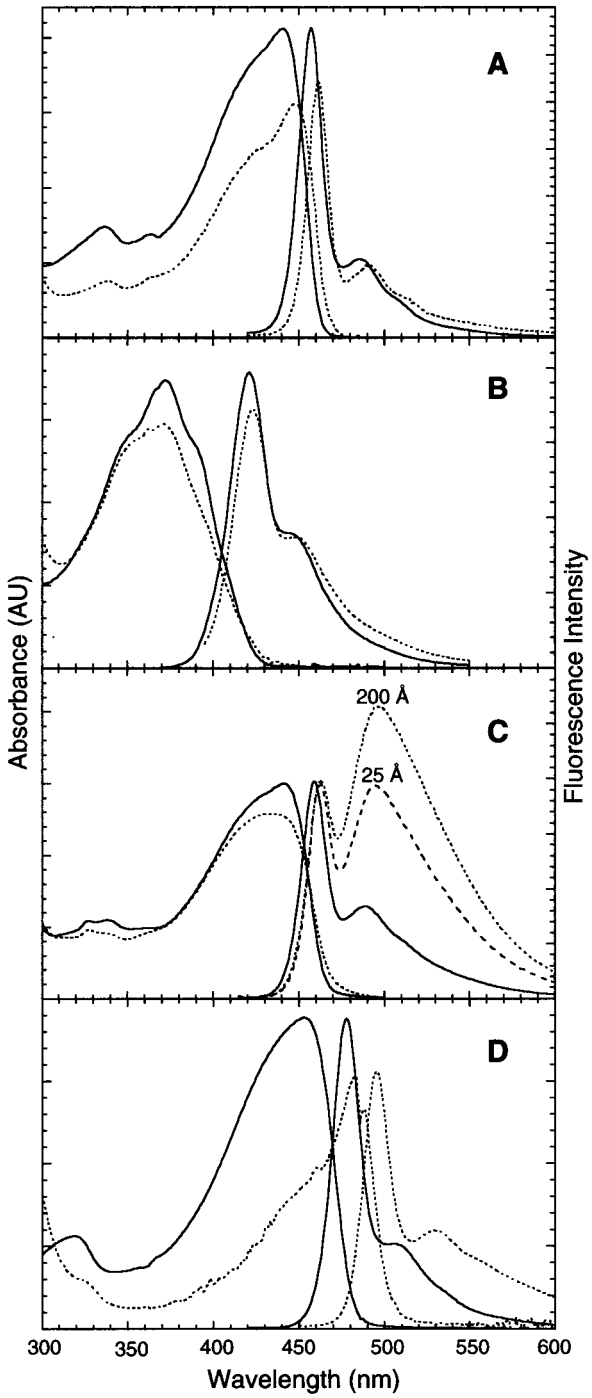

Figure 2. The absorption and fluorescence spectra of (A) **1**, (B) **2**, (C) **3**, and (D) **4** in dichloromethane (solid lines) and in spin-cast films (dotted lines).

in the thin films, the absorption band of **3** is broadened and slightly blue-shifted, as opposed to the small red shift observed for films of **1** relative to their solution spectra. On the basis of this information and the fact that a simple naphthalene−naphthalene excimer emits at a much shorter wavelength (~420 nm)[19] than the broad band for **3**, we attribute the broad band to an exciplex formed between the naphthalene moieties and adjacent polymer chains with significant ground-state interactions. The relative ground-state redox potentials of naphthalene (1.6 and −2.3 V vs SCE)[20] and the excited-state redox potentials

(18) For an example of the steric effect of substituents on polymer luminescence see: Berggren, M.; Inganäs, O.; Gustafsson, G.; Rasmusson, J.; Andersson, M. R.; Hjertberg, T.; Wennerström, O. *Nature* **1994**, *372*, 444.

(19) Yanagidate, M.; Takayama, K.; Takeuchi, M.; Nishimura, J.; Shizuka, H. *J. Phys. Chem.* **1993**, *97*, 8881.

(20) Kavarnos, G. J.; Turro, N. J. *Chem. Rev.* **1986**, *86*, 401.

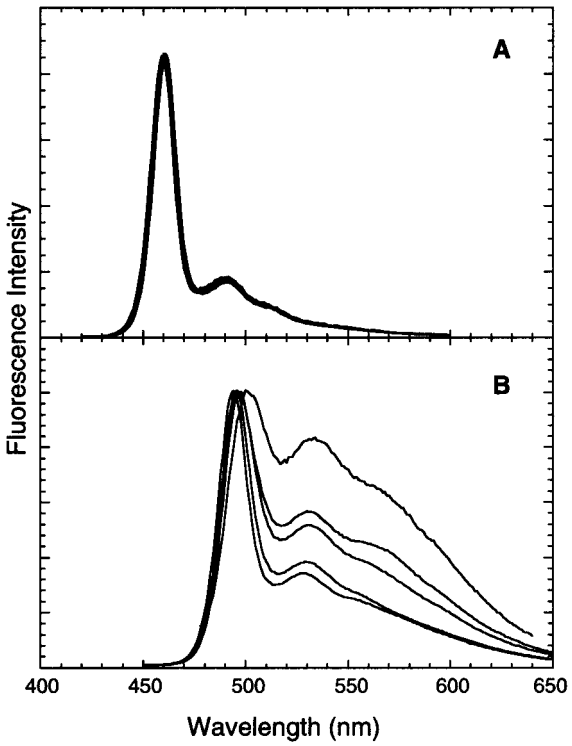

Figure 3. Overlay plot of the fluorescence spectra of (A) **1** and (B) **4** in five different spin-cast films.

of **3** (ca. 1.2 and −1.5 V vs SCE)[21] suggest that a charge-transfer state is not energetically favorable. It appears that the formation of exciplex in the films of **3** is a consequence of exciton resonance stabilization (excited energy delocalization).[22] As a result of the fluorescent exciplex formation, thin films of **3** show higher fluorescence quantum yield in the solid state than solution phase.

In contrast to pentiptycene-derived polymers **1**−**3**, which show little or no shift of the 0−0 absorption and emission bands in thin films, **4** displays substantial red shifts relative to solution values. This is consistent with our expectation that the rigid pentiptycene structure should prevent significant π-stacking interactions between polymer backbones. It is also interesting to note that all three pentiptycene-derived polymers have inherently higher solution fluorescence quantum yields than **4**. The difference of fluorescence efficiency of these pentiptycene-derived polymers vs **4** is even more significant in the solid state (Table 1). Aggregation of conjugated polymers has generally been responsible for decreased luminescence efficiencies,[23] and this process is of particular importance in electroluminescence. The high solubility of polymers **1**−**3** in organic solvents also reflects the reduced interpolymer interactions. For example, **1** is at least 100-fold more soluble than **4** in chloroform. The relative solubility of the polymers in chloroform is **1** $\sim$ **2** > **3** $\gg$ **4**, which is also in agreement with our spectroscopic interpretations based on the difference in absorption and fluorescence of polymer thin film vs solution spectra.

It appears that prevention of direct contact of the conjugated backbones also contributes to the greater spectroscopic stability and reproducibility of films of **1**−**3** relative to **4**. Figure 3 compares normalized fluorescence spectra of **1** and **4** in five spin-cast films of similar film thickness (20−30 Å) prepared under the same conditions. It is clear that the thin-film fluorescence spectrum of **4** is poorly reproducible, while films of **2** and **3**, similar to **1**, exhibit high spectroscopic reproducibility. Additionally, while the thin-film fluorescence spectra of **1**−**3** are stable under prolonged irradiation, a decrease of fluorescence intensity was observed in some films of **4**. The utility of the pentiptycene groups is even more apparent in the thermal and solvent stability of the polymer films. Fresh films of **1**−**3** exhibit little if any decrease (<25%) in fluorescence intensity when heated to 140 °C or when washed with methanol for 10 min. In contrast, with washing and heating **4** displays a large reduction of fluorescence (80%) and significant shape change in its absorption and emission bands. Such changes are presumably due to reorganization of the polymer chains. The enthalpic driving force for such reorganizations is expected to be smaller in cases for which the polymer backbones are not allowed to have direct co-facial π-contacts.

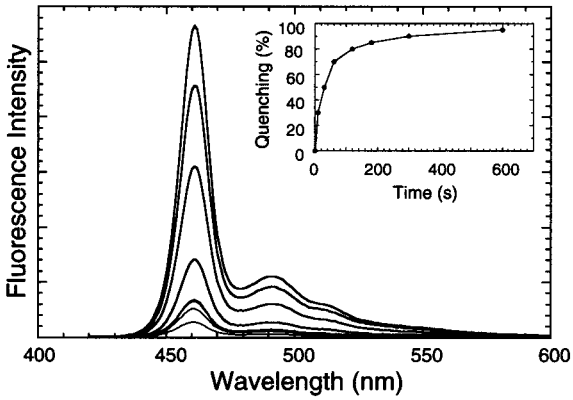

Figure 4. The time-dependent fluorescence intensity of **1** in a 25-Å film upon exposure to TNT vapor (room temperature) at 0, 10, 30, 60, 120, 180, 300, and 600 s (top to bottom), and the fluorescence quenching (%) as a function of time (inset).

Fluorescence Quenching Studies. The fluorescence response of polymer films to the vapors of various analytes was ascertained by inserting the polymer films into sealed vials (20-mL size) at room temperature containing solid (except for nitrobenzene, NB) analytes and cotton gauze, which prevents direct polymer analyte contact and helps to maintain a constant vapor pressure. The fluorescence spectra were recorded immediately after exposing the polymer films to analytes for a specific time. The quenching studies on polymers **1**, **2**, **3**, and **4** were performed with excitation wavelengths of 400, 360, 400, and 430 nm, respectively, and the analyte's equilibrium vapor pressures are assumed to be similar to the documented values.[24] The structures, relative vapor pressures (vs TNT, which is 8.02 $\times$ 10^{-6} mmHg or 10 ppb at 25 °C), and redox potentials[25] (vs SCE) of the analytes investigated are shown in Chart 2.

(a) Electronic and Structural Effects of Analytes. Figure 4 shows the time-dependent fluorescence intensity of **1** in a 25 $\pm$ 5 Å film (25-Å film hereafter) upon exposure to TNT vapor. The fluorescence quenching is 50 $\pm$ 5% at 30 s and increases to 70 $\pm$ 5 at 60 s (Figure 4, inset). The considerably faster response of the same film to DNT vapor (e.g. 75 $\pm$ 5% quenching at 10 s) can be attributed to the higher vapor pressure of DNT relative to TNT (18:1). The fluorescence quenching

(21) The reduction potentials (E_{red}) of polymers **1**−**3** estermated by CV are 1.22, 1.23, and 1.22, respectively. The 0−0 band energies (E_{0-0}) were used for the estimate of the oxdation potentials of their excited states.

(22) Gilbert, A.; Baggott, J. *Essentials of Molecular Photochemistry*; Blackwell Scientific Publications: London, 1991; Chapter 5.

(23) Cornil, J.; dos Santos, D. A.; Crispin, X.; Silbey, R.; Brédas, J. L. *J. Am. Chem. Soc.* **1998**, *120*, 1289.

(24) *Handbook of Physical Properties of Organic Chemicals*; Howard, P. H., Meylan, W. M., Eds.; CRC Press: Boca Raton, 1997.

(25) *Handbook Series in Organic Electrochemistry*; Meites, L., et al., Eds.; CRC Press: Boca Raton, 1978; Vol. 1.

Chart 2

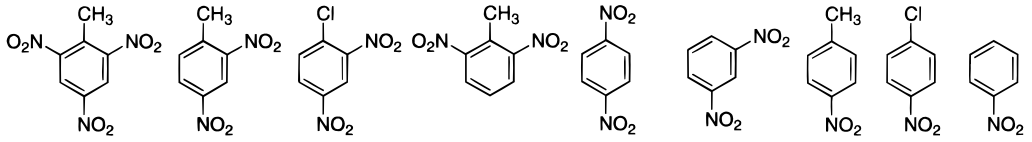

	TNT	DNT	CDNB	DNT*	pDNB	mDNB	NT	CNB	NB
rel. VP	1	18	10	70	3	110	2×10^4	3×10^3	3×10^4
E_{red} (V)	-0.7	-1.0	-0.8	-1.0	-0.7	-0.9	-1.2	-1.1	-1.15

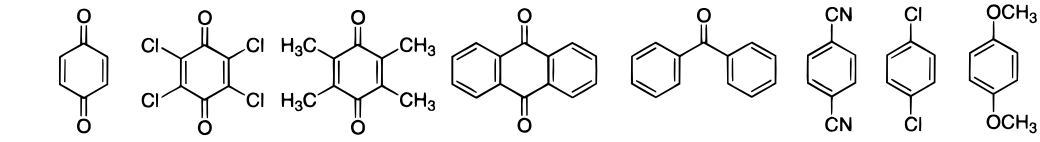

	BQ	CA	DQ	AQ	BP	DCNB	DClB	DMB
rel. VP	1×10^5	950	360	0.015	200	700	1×10^6	1×10^4
E_{red} (V)	-0.5	0.0	-0.8	-0.9	-1.6	-1.7	-1.8	< -2

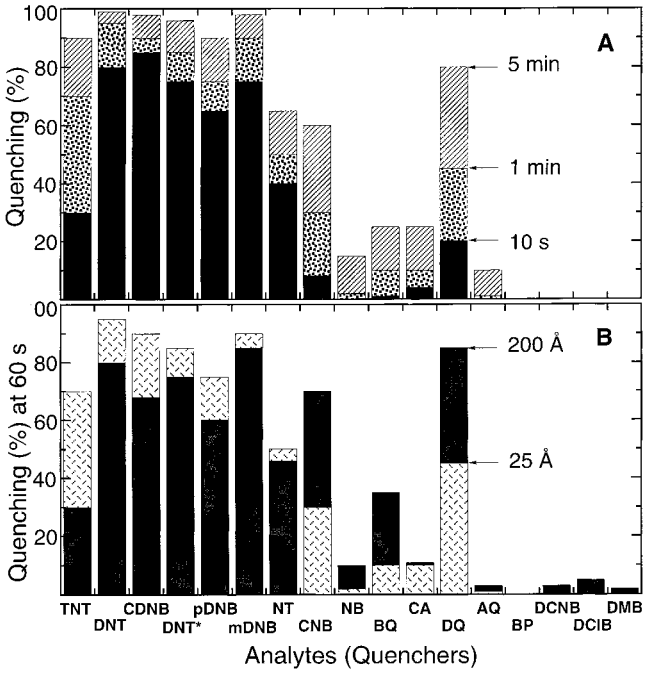

Figure 5. (A) The percent quenching of the fluorescence of **1** in 25-Å films by different analytes (quenchers) at room temperature with exposure times of 10 s, 1 min, and 5 min. (B) A comparison of the relative fluorescence quenching (%) of **1** in 25- vs 200-Å films at 60 s. The top of the solid bars indicates the quenching for a 200-Å film and the top of the crosshatched bars indicates the quenching in a 25-Å film.

(%) in 25-Å films of **1** to different analytes at 10 s, 1 min, and 5 min is depicted in Figure 5A. Overall, a significant response is only seen for nitro compounds (with the exception of NB) and duroquinone (DQ).

Several factors contribute to the observed fluorescence quenching. Since the mechanism of fluorescence attenuation is electron-transfer from the excited polymer to the analyte (oxidative quenching), the overall free energy change ($\Delta G°$) for an electron-transfer reaction must be considered.[19] In the case of oxidative quenching, this is approximated by

$$\Delta G° = E(\mathrm{P/P^{+\bullet}}) - \Delta E_{0-0} - E(\mathrm{Q/Q^{-\bullet}})$$

where $E(\mathrm{P/P^{+\bullet}})$, ΔE_{0-0}, and $E(\mathrm{Q/Q^{-\bullet}})$ are the redox potential of polymer $\mathrm{P} \rightarrow \mathrm{P^{+\bullet}}$, the lowest singlet 0−0 excitation energy of the polymer, and the redox potential of quencher $\mathrm{Q} \rightarrow \mathrm{Q^{-\bullet}}$, respectively. The fluorescence quenching (FQ) per unit time is affected by the vapor pressure (VP) of analytes, the exergonicity ($-\Delta G°$) of electron transfer, and the binding strength (K_b):

$$\mathrm{FQ} \propto (\mathrm{VP})[\exp(-\Delta G°)^2](K_b)$$

The values of $E(\mathrm{P/P^{+\bullet}})$ and ΔE_{0-0} for **1** are 1.22 V (vs SCE) and 2.74 eV, respectively. As a result, a zero or positive free energy change will result if the redox potential of the analyte ($E(\mathrm{Q/Q^{-\bullet}})$) is ≤ -1.52. In the cases of poor electron acceptors such as benzophenone (BP), dicyanobenzene (DCNB), dichlorobenzene (DClB), and dimethoxybenzene (DMB), unfavorable electron-transfer reactions ($\Delta G° \geq 0$) account for the absence of quenching (FQ = 0) despite the high vapor pressure (concentration) of these analytes. The low FQ for quinone species such as 1,4-benzoquinone (BQ) and chloranil (CA), which are excellent electron acceptors and have high vapor pressure, is likely the result of low polymer−quinone interactions (K_b). In this context, it is particularly interesting to compare the FQ of CA and DQ, since DQ shows a much larger quenching despite a lower VP and a smaller driving force ($-\Delta G°$). Chloro and methyl groups have similar size (van der Waals radii: 1.8 vs 1.7) and polarizability (12.3 for both)[26] but different charge distributions on their surface. Hence, CA and DQ exhibit a similar van der Waals size but different electrostatic interactions with the polymer film. Thus, the relatively lower FQ by CA indicates that electrostatic interactions are crucial in the binding event (K_b). The larger response to DQ vs CA is consistent with the positively charged surface created by the four methyl groups of DQ. The average charge on each of the 12 hydrogens in DQ was determined from a Mulliken population analysis (6-31G*) to be +0.19. Hence strong edge-to-face interactions between DQ and the electron-rich aromatic groups of the polymer films are possible. A similar analysis for CA shows each of the four chlorines to have a small charge

(26) *Handbook of Chemistry and Physics*; Lide, D. R., Ed.; CRC Press: Boca Raton, 1997.

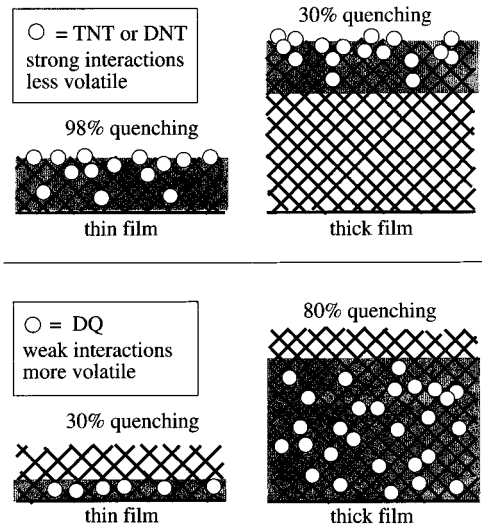

Figure 6. A schematic illustration of film-thickness effect (see text) on the fluorescence quenching displayed by nitro- and quinone-containing compounds.

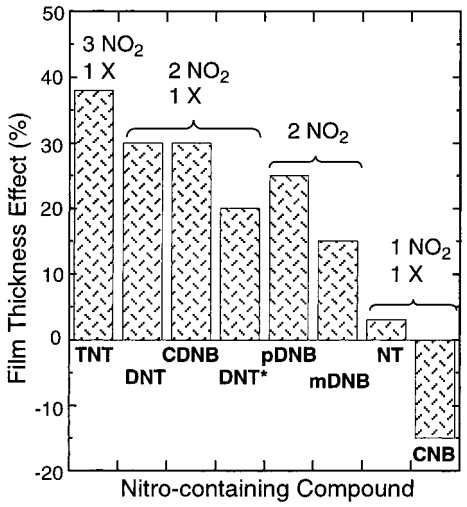

Figure 7. The film-thickness effect in the fluorescence quenching (%) of **1** in 25- vs 200-Å films for a series of nitro-containing compounds. A positive film-thickness effect indicates a higher quenching in a 25-Å film, similar to the situation described in Figure 6, top. Negative film-thickness effects are analogous to the situation in Figure 6, bottom.

(+0.12). On the other hand, we observe almost no difference in the fluorescence quenching of DNT and 1-chloro-2,4-dinitrobenzene (CDNB). This lack of discrimination can be attributed to a "leveling" effect by the two nitro substituents. Significant quenching for most of the nitro compounds, which have relatively lower VP and smaller $-\Delta G°$ than quinones, suggests strong interactions with the polymer films.

The dependence of fluorescence quenching on the thickness of polymer films can provide qualitative insight into the diffusion of analyte in the film. Consequently, we refer to the FQ as a measure of the percentage decrease in fluorescence intensity with respect to the virgin film. The 25-Å films of **1** correspond to only 2−3 layers of the polymer with its bulky pentiptycene groups (ca. 10-Å in width) on a glass substrate. Thus, these thin films can be quenched effectively with only surface-bound analytes, and the role of diffusion within the films is negligible in comparison to the other factors mentioned earlier. However, for a thicker 200-Å film, analytes having faster diffusion should distribute throughout the bulk of the film and in principle result in a larger FQ if all other factors are equal. Figure 5B shows the relative fluorescence quenching of **1** in 25- and 200-Å films at 60 s of exposure to analytes. While most of the nitro compounds have larger quenching in the 25-Å films, the other analytes in this study have larger quenching in the 200-Å films. In thicker films, the combination of slow diffusion of the nitro compounds into the interior of thicker films and the limited distance of energy migration (vide infra) produces lower FQ values. In contrast, the quinone species display larger FQ in thicker films, presumably due to their more facile diffusion throughout the polymer films. This effect, depicted in Figure 6, is also consistent with our belief that the three-dimensional pentiptycene scaffold provides porosity in thin films of **1**. Clearly, both the cavity size (steric hindrance) and the binding strength (relative polymer−analyte interactions) can affect the diffusion rate of analytes in a polymer film. Smaller cavities and stronger polymer−analyte interactions will result in slower diffusion. The cavities generated in spin-cast films of **1** are most likely a mixture of different sizes and shapes. The large quenching of DQ in 200-Å films (Figure 5B) indicates that there are cavities sufficiently large to allow the facile diffusion of molecules that have sizes less than or equal to that of DQ. Since the nitro compounds in this study have molecule sizes similar to or smaller than DQ, steric factors make only a minor contribution to the slow diffusion of these compounds in films of **1**. This suggests that the strong interactions (K_b values) of nitro compounds with the polymer films are responsible for their slow diffusion. In the case of the rapidly diffusing quinones, the greater number of cavities in 200-Å films leads to more effective sequestration (encapsulation) and, thus, a larger quenching. These film-thickness effects provide a useful criterion for the differentiation of nitro compounds from other species.

The difference in the FQ for 25- vs 200-Å films (called the film-thickness effect hereafter) can be used to provide a *qualitative* measure of the relative rate of diffusion of analytes in the polymer films. Specifically, a larger difference indicates a slower analyte diffusion rate, and a negative number means that the 200-Å films have larger quenching than 25-Å films. To further standardize the comparative quenching in 25- and 200-Å films, at least qualitatively, we need to take into account the mass transport of the analyte to the film, which is related to the vapor pressure. The time-dependent fluorescence quenching in 25-Å films suggests that a saturation stage (for which the response is not linear against exposure time) was reached at a quenching of around 80% (Figure 4, inset). Thus, the comparison of a relative film-thickness effect should be performed with an exposure time with no more than 85% FQ in a 25-Å film. For simplicity, a 10 s exposure time was chosen (Figure 5A) for all nitro compounds except for TNT, which required 60 s due to its slower response. Figure 7 shows this qualitative relationship; the more substituted nitro compounds, particularly those with more nitro substituents, display larger film-thickness effects. This result is again consistent with our expectation that compounds with multiple nitro substituents should have stronger electrostatic polymer−analyte interactions.

Studies on polymer **1** with shorter chain lengths (M_n = 43 vs 144 K, Table 1) reveal that the absorption and fluorescence spectra and the fluorescence quenching behavior are insensitive to molecular weight, thereby indicating that the conjugated polymer band gap is determined at very low degrees of polymerization. Similar FQs found for **1** with different molecular weights also confirms that the extent of energy migration and film morphologies are similar. It is know from studies in dilute solution that intrapolymer-chain energy migration is limited by the excited-state lifetime, the molecular weight of

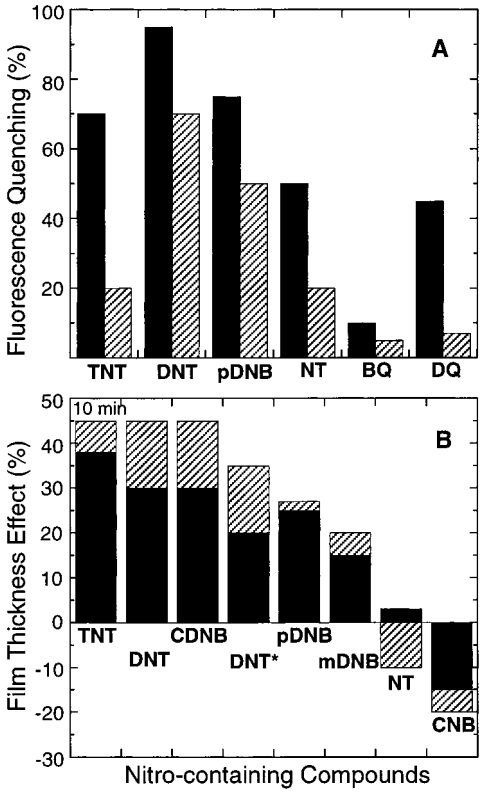

Figure 8. A comparison of (A) relative fluorescence quenching and (B) relative film-thickness effect of **1** (filled) and **2** (slashed) at 60 s (except for TNT at 10 min).

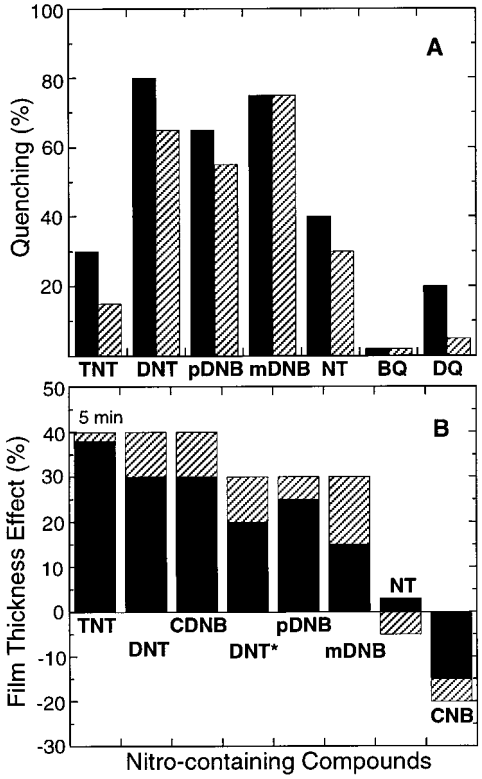

Figure 9. A comparison of (A) relative fluorescence quenching and (B) relative film-thickness effect of **1** (filled) and **3** (slashed) at 10 s.

the polymer, and the electron delocalization.[3] In films, the participation of interpolymer-chain energy migration can diminish the chain length dependence on energy migration. Energy migration is present in the polymer thin films as evidenced by fluorescence polarization measurements before and after exposure to TNT for 5 min (anisotropy = 0.01 and 0.35, respectively). The lack of polarization in the initial films indicates that extensive energy migration occurs. The increase of anisotropy after exposure to TNT indicates that greater spatial diffusion of the excitations, which would ordinarily lead to greater depolarization, increases the probability of quenching by TNT. The presence of facile energy migration produces a more dramatic (amplified) FQ response than would be observed in an isolated small molecule system.

(b) Electronic and Structural Effects of Polymers. To additionally probe polymer−analyte electrostatic interactions we have varied the electronic properties of the polymer. Due to the electron-withdrawing character of amide groups, polymer **2** is expected to have weaker electrostatic interactions with electron-deficient analytes and, in turn, smaller fluorescence quenching. Indeed, **2** exhibits relatively smaller fluorescence response to oxidative quenchers than **1**. Figure 8A shows the quenching of **1** and **2** by several representative analytes with an exposure time of 60 s. On the basis of purely electronic considerations, we expected that weaker interactions between **2** and electron-poor analytes should lead to a smaller film-thickness effect in **2** relative to **1**. However, as seen in Figure 8B, this is only true for small molecules such as NT and CNB, whereas molecules such as TNT, DNT, and CDNB exhibit a larger film-thickness effect for **2**. This result indicates that the larger steric hindrance in **2** produces slower rates of diffusion for the larger compounds. In other words, due to the amide groups having a nonplanar structure and a doubling of the alkyl chains, the cavity size in **2** is on average smaller than those of **1**. Recall also that a different equilibrium polymer conformation, which will also impact the cavity size of **2**, was suggested by the blue-shift in the absorption and fluorescence spectra of thin films relative to solution.

The structural (cavity size) effects can also be tested by comparing **1** and **3**, which have similar electronic structures, but different film morphologies due to an extension of the pentiptycene groups in **3**. Figure 9 shows the relative fluorescence quenching with a short (10 s) exposure to representative quenchers in 25-Å films and shows the film-thickness effects between 25- vs 200-Å films. The similar quenching in 25-Å films shows that both **1** and **3** exhibit similar binding constants. The observed film-thickness effects (Figure 9B) indicate restricted diffusion due to smaller cavities in **3** relative to **1**. A smaller cavity size is also in agreement with the interpolymer interactions in **3**, as discussed previously to explain the solubility and spectroscopic data. As such, the smaller size of cavities in **3** may also be responsible for the slightly smaller fluorescence quenching in cases of TNT, DNT, and DQ (Figure 9A).

In comparison to pentiptycene polymers **1**−**3**, polymer **4**, with double the alkoxy groups and the most electron-rich structure, shows the least fluorescence quenching toward electron-deficient analytes (e.g., FQ for ∼30-Å films and 60-s exposure is 20% for TNT, 60% for DNT, and <10% for DQ). This result is consistent with the lack of porosity in films of **4**, as is suggested from its planar structure and the spectroscopic studies (Figure 2D). The poor solubility of **4** in organic solvents prevented us from studying its film-thickness effect. In short, unsatisfactory spectroscopic stability and reproducibility indicates that **4** is not a good candidate as a fluorescent chemosensor.

Concluding Remarks

The degree of fluorescence quenching of polymer films by analytes depends on a variety of factors, including the vapor

pressure, the exergonicity of electron transfer, the binding strength (polymer−analyte interactions), and the diffusion ability of analytes through polymer films. Our analysis of these interrelated properties has helped to elucidate important features that determine the sensitivity of polymers **1**−**3** to various analytes. The molecular recognition properties are mainly governed by the electrostatic interactions between the electron-rich polymers and electron-deficient analytes. In this regard, we have shown the electron-rich environment of the polymer films to be crucial. Our data suggest that a good balance of electrostatic interactions and film porosity is the key to produce a TNT optical sensor with high sensitivity. Among them, the film morphology seems most important because films with large cavities favor TNT binding and diffusion. However, the film morphology is difficult to control as shown by the comparisons of **3** and **1**. In fact, we initially designed **3**, which has an extended ring system in its pentiptycene moieties, to display a larger cavity size in the film. However, due to the unexpected interpolymer interactions between naphthalenoid pentiptycenes and adjacent polymer backbones, the average cavity size in **3** appears to be smaller than that of **1**. Different approaches are necessary for tailoring the film porosity. Additionally, we have shown a variety of differential responses to the same analytes by varying the polymer's structure and thickness. These relationships can be used to create a sensory array for the formation of a reliable (selective) TNT detector. Efforts toward this goal and the synthesis of more elaborate systems are ongoing in our laboratory.

Experimental Section

General Methods. NMR (^{1}H and ^{13}C) spectra were recorded on 250, 300, or 500 MHz spectrometers, and chemical shifts are reported in ppm relative to TMS in proton spectra and to $CHCl_3$ in carbon spectra. Elemental analyses were performed by Desert Analytics Laboratory, Tucson, AZ. The molecular weights of polymers were determined by using a PLgel 5 μm Mixed-C (300 × 7.5 mm) column and a diode array detector at 254 nm at a flow rate of 1.0 mL/min in THF. The molecular weights were reported relative to polystyrene standards purchased from Polysciences, Inc. Polymer thin films on a cover glass (18 × 18 mm) were spin cast by a EC101DT photo resist spinner (Headway Research, Inc), using a spin rate of 3000 rpm from chloroform solutions, and placed under vacuum overnight before use. To generate a 25-Å film generally requires 1 mg of polymer in 2 mL of chloroform. The film thickness was determined for samples prepared on both silicon wafers and cover glasses. The former was subject to ellipsometric measurement with a L125B system (Gaertner Scientific Corporation) and the latter was used to obtain optical density. An excellent linear relationship of ellipsometric data and optical density (OD) was established with films thicker than ca. 60 Å and this allows the film thickness to be estimated by OD in cases where the polymer film is thinner than 60 Å. UV−vis spectra were obtained from a Hewlett-Packard 8452A diode array spectrophotometer. Mass spectra were determined with a Finnigan MAT 8200 system using sector double focus and an electron impact source with an ionizing voltage of 70 V. The X-ray crystal structure was determined with a Siemens SMART/CCD diffractometer. Melting points were determined on a Perkin-Elmer DSC 7 system. The redox potentials of polymers were determined by cyclic voltammetry (CV) in 0.1 M Bu_4NPF_6/CH_2Cl_2 solutions on a platinum button electrode with a platinum coil auxiliary electrode and an isolated silver/silver nitrate reference electrode using an EcoChemie Autolab potentiostat. The data were corrected by the CV of ferrocene under the same conditions. Quantum chemical calculations were performed with the MacSpartan program. Geometries were first optimized initially at the AM1 level. The final geometries were then optimized with 6-31G* level calculations. Column chromatography was performed on 40 μm silica gel (Baker).

Fluorescence studies were conducted with a SPEX Fluorolog-τ2 fluorometer (model FL112, 450 W xenon lamp) equipped with a model 1935B polarization kit. Polymer thin-film spectra were recorded by front-face (22.5°) detection. Monochromators were corrected by lamp output and a water Raman scan. Fluorescence quantum yields in methylene chloride solution and polymer films were determined relative to equiabsorbing solutions of anthracene ($\Phi_F = 0.27$ in hexane)[27] and films of ∼10−3 M 9,10-diphenylanthracene in poly(methyl methacrylate) (PMMA)($\Phi_F = 0.83$),[28] respectively. The time decay of fluorescence was determined by a phase-modulation method,[29] using frequencies from 10 to 310 MHz.

Materials. All solvents were spectral grade (EM sciences or Mallinckrodt) unless otherwise noted. Anhydrous toluene, THF, and diisopropylamine were purchased from Aldrich Chemical Co, Inc. TNT was obtained from Sandia National Laboratory. All other compounds including analytes (Aldrich) were used as received. 1,4-Bis(tetradecyloxy)-2,5-diiodobenzene (**5**)[10] and 1,4-bis(*N*,*N*-dioctylcarbamoyl-2,5-diiodobenzene (**6**)[3] were synthesized according to the literature procedures.

Iptycene Quinones 9 and 10. To a mixture of anthracene (17.8 g, 0.1 mol) and benzoquinone (5.4 g, 0.05 mol) in a 200-mL round-bottomed flask fitted with a condenser was added 75 mL of mesitylene. The mixture was refluxed for 24 h and then the solid was filtered after cooling to room temperature. The hydroquinone solid was digested in 100 mL of hot xylene twice and filtered (16.5 g). The crude hydroquinones (8 g) were dissolved in hot glacial acetic acid (ca 300 mL) and then a solution of 1.5 g of potassium bromate (9 mmol) in 100 mL of hot water was added. A deep orange color and precipitate developed immediately. The solution was boiled for a few minutes and then an additional 100 mL of hot water was added and the heat was removed. The orange quinone solid was collected after the solution was cooled. The quinones were washed with acetic acid and then with water. The crude quinones were dissolved in chloroform (ca. 120 mL) and washed with sodium bicarbonate and brine. The organic layer was separated and dried ($MgSO_4$). The dark-colored impurities were removed by filtering the chloroform solution through a thin layer of silica gel. The resulting orange solution was adsorbed onto ca. 50 g of silica gel. The resulting yellow silica gel solid mixture was chromatographed with hexane/ethyl acetate (5:1) as the eluent to obtain compound **9** in 80−95% purity, which can be further purified by column chromatography with pure chloroform as the eluent. Compound **10** stays bound to the silica gel and was obtained as a pure material by extraction of the silica gel with chloroform. The overall yields for **9** and **10** were 13% and 39%, respectively. **9** (mp 294.0 °C, lit. mp 292−296 °C): ^{1}H NMR (250 MHz, $CDCl_3$) 5.80 (s, 2H), 6.60 (s, 2H), 7.04 (dd, J = 3.3 and 5.3 Hz, 4H), 7.43 (dd, J = 3.3 and 5.3 Hz, 4H) ppm; ^{13}C NMR (75 MHz, $CDCl_3$) 47.36, 124.40, 125.56, 135.36, 143.57, 151.90, 183.48 ppm. **10** (mp >350 °C, lit. mp >370 °C): ^{1}H NMR (250 MHz, $CDCl_3$) 5.75 (s, 4H), 6.97 (dd, J = 3.2 and 5.3 Hz, 8H), 7.36 (dd, J = 3.2 and 5.3 Hz, 8H) ppm; ^{13}C NMR (75 MHz, $CDCl_3$) 47.39, 124.24, 125.46, 143.65, 150.95, 179.96 ppm.

Iptycene Quinones 11−13. A mixture of pentacene (0.96 g, 3.45 mmol) and quinone **9** (1.27 g, 4.49 mmol) in 3 mL of toluene was refluxed for 3 days and then cooled. The resulting yellow solid (1.87 g) was filtered and washed with hexane. The solid was placed in a round-bottom flask and ca. 80 mL of glacial acetic acid was added, then the solution was heated to reflux and 5−10 drops of HBr (48%) was added. The color of solution faded in a short period of time. The solution was cooled after 30 min and then any undissolved solid was filtered off. The filtrate was then reheated again and potassium bromate (0.3 g in 20 mL of hot water) was added. The solution was boiled for a few minutes, an additional 10 mL of hot water was added, and the heat was removed. The orange quinone solid was collected and washed with acetic acid and water. Column chromatography with pure chloroform as eluent allowed the separation of **13** from the mixture of **11** and **12**, which can be separated by another column chromatography with a mixed solvent of chloroform and hexane (2:1). **11** (mp 408 °C): ^{1}H NMR (250 MHz, $CDCl_3$) 5.77 (s, 2H), 5.96 (s, 2H), 6.94 (dd,

(27) Birks, J. B. *Photophysics of Aromatic Molecules*; Wiley-Interscience: London, 1970.
(28) Osaheni, J. A.; Jenekhe, S. A. *J. Am. Chem. Soc.* **1995**, *117*, 7389.
(29) Hieftje, G. M.; Vogelstein, E. E. *Modern Fluorescence Spectroscopy*; Wehry, E. L., Ed.; Plenum Press: New York, 1981.

J = 3.1 and 5.3 Hz, 4H), 7.33−7.39 (m. 8H), 7.67 (dd, J = 3.3 and 6.1 Hz, 4H), 7.81(s, 4H) ppm; ^{13}C NMR (125 MHz, $CDCl_3$) 46.34, 47.38, 122.89, 124.23, 125.43, 126.18, 127.53, 131.68, 139.08, 143.55, 149.21, 151.16, 180.11 ppm; MS *m*/*z* (relative intensity) 560 (M^+, 100), 561 ($M^+ + 1$, 45), 562 ($M^+ + 2$, 10); HRMS calcd for $C_{42}H_{24}O_2$ (M^+) 560.1776, found 560.1769. **12** (mp 429 °C): ^{1}H NMR (250 MHz, $CDCl_3$) 5.79 (s, 2H), 5.97 (s, 2H), 6.91(dd, J = 3.2 and 5.4 Hz, 2H), 6.98 (dd, J = 3.1 and 5.4 Hz, 2H), 7.07 (dd, J = 3.3 and 5.4 Hz, 2H), 7.33 (dd, J = 3.1 and 5.4 Hz, 2H), 7.38 (dd, J = 3.3 and 5.3 Hz, 2H), 7.47 (dd, J = 3.1 and 5.4 Hz, 2H), 7.55 (dd, J = 3.1 and 6.8 Hz, 2H), 8.45 (dd, J = 3.3 and 6.7 Hz, 2H), 8.46 (s, 2H) ppm; ^{13}C NMR (125 MHz, $CDCl_3$) 46,47, 47.40, 122.75, 123.05, 124.27, 124.28, 124.64, 125.46, 125.50, 126.35, 127.34, 128.16, 129.55, 131.15, 140.75, 141.94, 143.44, 143.56, 149.07, 151.27, 179.91 ppm; MS *m*/*z* (relative intensity) 716 (M^+, 39), 718 ($M^+ + 2$, 100), 720 ($M^+ + 4$, 68); HRMS calcd for $C_{42}H_{22}O_2Br_2$ (M^+) 715.9987, found 715.9987. Anal. Calcd for $C_{42}H_{22}O_2Br_2$: C, 70.22, H, 3.09. Found: C, 69.84, H, 3.28. **13** (mp >400 °C): ^{1}H NMR (250 MHz, $CDCl_3$) 5.60 (s, 4H), 5.67 (s, 4H), 6.88 (dd, J = 3.1 and 5.4 Hz, 8H), 6.93 (dd, J = 3.2 and 5.4 Hz, 4H), 7.24−7.33 (m. 12H), 7.38 (s, 2H); ^{13}C NMR (125 MHz, $CDCl_3$) 47.09, 47.23, 120.81, 124.11, 124.19, 125.32, 125.41, 141.66, 143.47, 143.50, 143.61, 150.76, 150.98, 179.71; MS *m*/*z* (relative intensity) 842 (M^+, 100), 723 ($M^+ + 1$, 20); HRMS calcd for $C_{62}H_{34}O_4$ (M^+) 842.2457, found 842.2458.

Compounds 14 and 15. A general procedure is illustrated by the synthesis of **14**. Under an atmosphere of argon, 1 equivalent of *n*-butyllithium (2.5 mmol) in hexane was added dropwise to a solution of (trimethylsilyl)acetylene (0.35 mL, 2.5 mmol) in THF at 0 °C. The mixture was then kept at 0 °C for another 40 min before it was transferred to a solution of quinone **10** (0.46 g, 1 mmol) in THF at 0 °C. The mixture was warmed to room temperature and stirred overnight. The reaction was quenched with 1 mL of 10% HCl and then subjected to a $CHCl_3/H_2O$ workup. The solvent was removed and hexane was then added to the residue. The resulting white solid (0.59 g, 90%, 0.90 mmol), which is a mixture of the trans and cis isomers, was collected by filtration. This crude solid was dissolved in 10 mL of acetone and then a solution of tin(II) chloride dihydrate (0.51 g, 2.25 mmol) in 50% of acetic acid (10 mL) was added dropwise. This mixture was stirred at room temperature for another 24 h and the resulting solid product was filtered. The solid was then dissolved in $CHCl_3$ and washed with water and sodium bicarbonate and then dried ($MgSO_4$). The $CHCl_3$ was removed in vacuo and the residue was washed with hexane to remove the yellow impurities. The resulting white solid was collected (yield 85%). **14** (mp 419 °C): ^{1}H NMR (250 MHz, $CDCl_3$) 0.51 (s, 18H), 5.80 (s, 4H), 6.96 (dd, J = 3.2 and 5.3 Hz, 8H), 7.36 (dd, J = 3.2 and 5.3 Hz, 8H) ppm; ^{13}C NMR (62.5 MHz, $CDCl_3$) 0.31, 52.2, 100.7, 102.5, 114.8, 123.8, 125.2, 144.1, 144.9 ppm; MS *m*/*z* (relative intensity) 622 (M^+, 100), 623 ($M^+ + 1$, 56), 624 ($M^+ + 2$, 24); HRMS calcd for $C_{44}H_{38}Si_2$ (M^+) 622.2512, found 622.2513. **15** (mp 366.6 °C): ^{1}H NMR (250 MHz, $CDCl_3$) 5.80 (s, 2H), 6.02 (s, 2H), 6.90 (dd, J = 3.2 and 5.3 Hz, 4H), 7.29−7.35 (m, 8H), 7.66 (dd, J = 3.3 and 6.1 Hz, 4H), 7.77 (s, 4H) ppm; ^{13}C NMR (125 MHz, $CDCl_3$) 0.39, 51.44, 52.20, 100.48, 102.91, 114.92, 122.07, 123.77, 125.20, 125.69, 127.45, 131.89, 140.84, 142.50, 144.67, 144.86 ppm; MS *m*/*z* (relative intensity) 722 (M^+, 100), 723 ($M^+ + 1$, 62), 724 ($M^+ + 2$, 28); HRMS calcd for $C_{52}H_{42}Si_2$ (M^+) 722.2825, found 722.2825. Anal. Calcd for $C_{52}H_{42}Si_2$: C, 84.83, H, 6.15. Found: C, 84.61, H, 6.02.

Compounds 7 and 8. The deprotection of the trimethylsilyl group was carried out by dissolving compounds **14** or **15** in a mixture of KOH (two tablets in 1 mL of H_2O), THF, and MeOH and stirring at room temperature for 5 h. The resulting solid product was filtered and washed with water and then dried in vacuo. **7** (mp 439.5 °C): ^{1}H NMR (300 MHz, $CDCl_3$) 3.69 (s, 2H), 5.82 (s, 4H), 6.95 (dd, J = 3.2 and 5.4 Hz, 8H), 7.36 (dd, J = 3.2 and 5.4 Hz, 8H) ppm; MS *m*/*z* (relative intensity) 478 (M^+, 100), 479 ($M^+ + 1$, 32); HRMS calcd for $C_{38}H_{22}$ (M^+) 478.1722, found 478.1720. **8** (mp >300 °C); ^{1}H NMR (250 MHz, $CDCl_3$) 3.79 (s, 2H), 5.85 (s, 2H), 6.07 (s, 2H), 6.91 (dd, J = 3.1 and 5.3 Hz, 4H), 7.32−7.36 (m. 8H), 7.67 (dd, J = 3.3 and 6.1 Hz, 4H), 7.82 (s, 4H) ppm; ^{13}C NMR (125 MHz, $CDCl_3$) 51.24, 51.98, 78.96, 84.92, 114.13, 122.18, 123.83, 125.31, 125.75, 127.47, 131.90, 140.63, 143.12, 144.51, 145.35 ppm; MS *m*/*z* (relative intensity) 578 (M^+, 100), 579 ($M^+ + 1$, 38), 580 ($M^+ + 2$, 11); HRMS calcd for $C_{46}H_{26}$ (M^+) 578.2035, found 578.2034.

Polymers 1−3. A general procedure is illustrated by the synthesis of polymer **1**. Under an atmosphere of argon, diisopropylamine/toluene (2:3, 2.5 mL) solvent was added to a 25-mL Schlenk flask containing compound **7** (40 mg, 0.084 mmol), 1,4-bis(tetradecanyloxyl)-2,5-diiodobenzene (63 mg, 0.084 mmol), CuI (10 mg, 0.053 mmol), and $Pd(Ph_3)_4$ (10 mg, 0.0086 mmol). This mixture was heated at 65 °C for 3 days and then subjected to a $CHCl_3/H_2O$ workup. The combined organic phase was washed with NH_4Cl water, and then dried ($MgSO_4$). The solvent was removed in vacuo, and the residue was reprecipitate in methanol three times. The polymer was a yellow solid (76 mg, 75%). **1**: ^{1}H NMR (250 MHz, $CDCl_3$) 0.87 (br, 6H), 1.23 (br, 36H), 1.46 (br, 4H), 1.73 (br, 4H), 2.23 (br, 4H), 4.47 (br, 4H), 6.11 (br, 4H), 7.03 (br, 8H), 7.44 (br, 2H), 7.50 (br, 8H). **2** (85%) ^{1}H NMR (250 MHz, $CDCl_3$) 0.65−1.42 (br m, 52 H), 1.65 (br, 8H), 3.45 (br, 8H), 5.91 (br, 4H), 7.02 (br, 8H), 7.42 (br, 4H), 7.58 (br, 4H), 7.87 (br, 2H). **3** (82%): ^{1}H NMR (250 MHz, $CDCl_3$) 0.87 (br, 6H), 1.20 (br, 36H), 1.50 (br, 4H), 1.81 (br, 4H), 2.35 (br, 4H), 4.60 (br, 4H), 6.17 (br, 2H), 6.39 (br, 2H), 7.05 (br, 4H), 7.20−7/70 (br, 10H), 7.78 (br, 4H), 7.98 (br, 4H).

Acknowledgment. The authors gratefully acknowledge financial support from The Office of Naval Research and The Defense Advanced Research Projects Agency for funding. Additional appreciation is due to Professor M. G. Bawendi for the use of his spin coater, Dr. William Davis for resolving the crystal structure of **14**, Mr. Sean McHugh, who generously supplied polymer **4**, Dr. Dan Fu for the supply of monomer **6**, Mr. Jinsang Kim for the help of determining film thickness, Mr. Richard Kingsborough for CV measurements, and Dr. Vance Williams for helpful discussions.

Supporting Information Available: Tables of detailed fluorescence quenching data for polymers **1**−**3** and the crystallographic data of compound **14** and NMR (^{1}H and ^{13}C) spectra of compounds **1**−**3**, **7**, **8**, and **11**−**15** (31 pages, print/PDF). See any current masthead page for ordering information and Web access instructions.

JA982293Q